Journal of Communication Engineering (JCE)

P- ISSN: 2322-4088 Vol. 12, No. 1, Jan.-Jun. 2023 E- ISSN: 2322-3936

Accurate Sensing with Dual-band Absorber Based on Graphene Doped Lattice for Terahertz Frequencies

M. Ghaderi Electrical And Computer Engineering Faculty; Semnan University; Semnan, Iran;
Email: m.ghaderi@alum.semnan.ac.ir

Pejman Rezaei* **[Corresponding Author]** Electrical And Computer Engineering Faculty; Semnan University; Semnan, Iran;
Email: prezaei@semnan.ac.ir

Received: *11 Dec. 2022* ***Revised:*** *05 Feb. 2023* ***Accepted:*** *13 Mar. 2023*

Abstract: Dual-band absorbers using identical shaped graphene doped lattice, with high absorbance coefficients are investigated in this paper. A dynamically tunable dual-band terahertz metamaterial absorber is proposed based on a hybrid graphene-doped frequency selective surface (FSS) structure. The unit cell incorporates concentric square graphene ring resonators and a planar graphene sheet sandwiched between dielectric layers, supported by a metallic backing. These resonators are responsible for the resonance effect and enable dual-band operation. By adjusting the chemical potential of graphene through external gate voltage, the absorption peaks can be dynamically tuned, demonstrating strong spectral flexibility. Simulation results show a maximum absorption of 99.63% at 32.42 THz. Additionally, the impact of different dielectric substrates on the tunability and bandwidth separation is studied, revealing further structural reconfigurability. The proposed absorber also maintains high absorption efficiency under oblique incidence, indicating robust angular stability. These features make the structure a strong candidate for advanced THz sensing and stealth applications.

Index Terms: Graphene Doped, Ring Resonator, Frequency Selective Surface, Terahertz Metasurfaces, Absorption Coefficient, Tunable Absorber.

Citation: M. Ghaderi and Pejman Rezaei, "Accurate Sensing with Dual-band Absorber Based on Graphene Doped Lattice for Terahertz Frequencies," *Journal of Communication Engineering*, vol. 12, no. 1, pp. 35-46, Jan.-Jun. 2023.
http://dx.doi.org/10.22070/jce.2025.20085.1279

I. INTRODUCTION

Photonics comes from "photon" which is everything related to light including generation, amplification, transmission, absorption, modulation, and detection of light [1-5]. Photonic crystals [6-9], plasmonics [10-12], and graphene-based structures [13-16] are commonly employed as optic materials at THz frequencies.

The energy dispersion diagram of graphene is without a band gap and just like a conductor. Graphenes conductivity, in the absence of electromagnetic bias, is simply a scalar value. Therefore, under static electromagnetic conditions, graphene's conductivity can be represented by a tensor. Applying bias to graphene results in gyro-tropic and nonreciprocal characteristics [17-22].

As a result, the conductivity of graphene displays nonisotropic and is a complex number, with both real and imaginary components varying depending on frequency [23-25]. Graphene periodic structures can be assumed as 2D metasurfaces that have the ability to diffraction of incident waves. The conductivity of graphene material is interdependent on the chemical potential, and can be modified with an external bias voltage. Since, these structures have many applications in optic lenses, antennas, phase shifters, and absorbers [26, 27]. Only a singular graphene sheet displays an absorbing ability of approximately 2.3%. However, a doped graphene film demonstrates full absorbance. Consequently, various configurations of graphene patches and slotted array sheets are utilized in absorber designs at THz frequencies [28].

Graphene Frequency Selective Surfaces (FSS) consist of an infinite periodic array of patches or apertures on a dielectric substrate, and can be used as THz absorbers. Electromagnetic wave absorbers are being used to prevent the visibility of objects and minimize interferences. The classification of absorbers as resonant or broadband depends on the intended applications. Various types of resonant absorbers include single, dual, and multi-band absorbers designed for a range of frequencies, from microwaves to optical applications. Graphene FSS metasurfaces are used for THz applications with narrow bandwidth or broadband absorption [29-34]. In this paper, a novel THz dual-band absorber with a simple unit cell of FSS structure is presented. Different gate voltages changed the chemical potential of graphene, resulting in varied absorption frequencies. Furthermore, various substrate permittivity variations impact absorption frequencies, examined in this study.

In [35], a single-band absorber based on graphene metamaterial presented with excellent absorption of 99.99% at 7.628 THz. A quad-band perfect absorber is introduced in [36]. At four separate frequencies, 2.7 THz, 3.19 THz, 3.99 THz, and 4.46 THz, absorptions reaching an average of 99.43% can be attained. In [37] A novel absorber design using a single graphene circular ring on dielectric spacer unit cells placed on a continuous metallic film, was suggested for achieving

absorption in both single and dual bands. The average absorption is 99% provided at 210.2 THz, 227.3 THz, 297.7 THz, and 337.4 THz.

In this research, graphene layer absorption characteristics are taken into account for getting better absorption. In other words, the FSS absorbers, which consist of periodic multilayer unit cells, are specified in such a way that the absorption characteristics are enhanced. Unit cells consist of identical graphene patches on the substrate with a continuous graphene layer with an entirely metal layer placed at the bottom to increase the absorption. Unique initial properties of graphene influenced absorber quality, as variations in the chemical potential of the graphene layer affected the absorption spectrum.

II. GRAPHENE NANOPARTICLES DESIGN

The Graphene structure consists of a one layer of carbon atoms organized in a regular honeycomb lattice structure. In this material, a complex conductivity can be continuously tuned in a broad frequency range by shifting the electronic Fermi level via chemical or electronic doping, temperature T, and frequency of incident wave.

The real, σ_r, and imaginary parts of the graphene conductivity, σ_i, are calculated from Kubo expressed by Equations 1, 2 [38, 39].

$$\sigma_r = \frac{H\sigma_0}{2}\left[tanh\left(\frac{\hbar\omega+2\mu_c}{4k_BT}\right) + tanh\left(\frac{\hbar\omega-2\mu_c}{4k_BT}\right)\right] \quad (1)$$

$$\sigma_i = \frac{4\mu_c}{\hbar\omega}\frac{\sigma_0}{\pi}\left(1-\frac{2\mu_c^2}{9t^2}\right) - \frac{H\sigma_0}{\pi} log\frac{|\hbar\omega+2\mu_c|}{|\hbar\omega-2\mu_c|} \quad (2)$$

Where $\sigma_0 = \frac{e^2}{4\hbar}$ and $H = \left[1+\frac{(\hbar\omega)^2}{(36t^2)}\right]$, k_B is Boltzmann's constant, μ_c is the chemical potential, $\hbar$ is the reduced Plank's constant, ω is the angular frequency, and T is the temperature hopping parameter.

The density of carriers, μ_c, is controlled by changing the gate voltage between the graphene layer and the substrate.

The proposed absorber consists of multi-layered unit cells, including two graphene square rings on top of the dielectric. A planar graphene sheet was placed on another dielectric substrate to increase the absorption. Additionally, a metal film sheet was placed on the bottom of the structure, as shown in Fig. 1.

The structure is optimized on a 400 nm dielectric layer with ε_r = 12 (dielectric 2). Another dielectric layer with ε_r = 2 and 10 nm thickness is used to separate two graphene layers (dielectric 1) independently. On the top layer, there are two graphene square rings in each unit cell. The width of each ring is $\boldsymbol{t}$ = 4.5 nm. The outside length of the outer square ring is $\boldsymbol{a}$ = 45 nm, and the outside

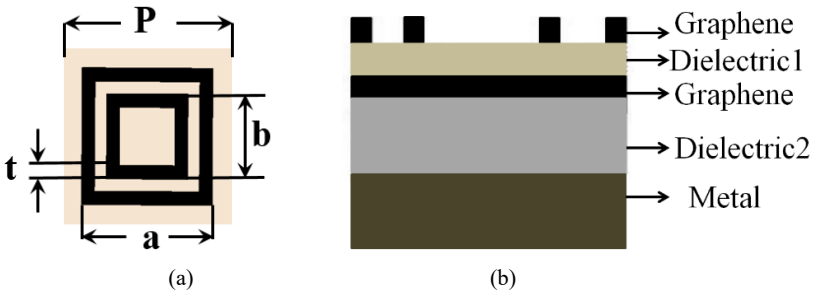

Fig. 1. Unit cell of proposed dual-band THz absorber. a top view of the graphene particles, b cross-section of the absorber layers

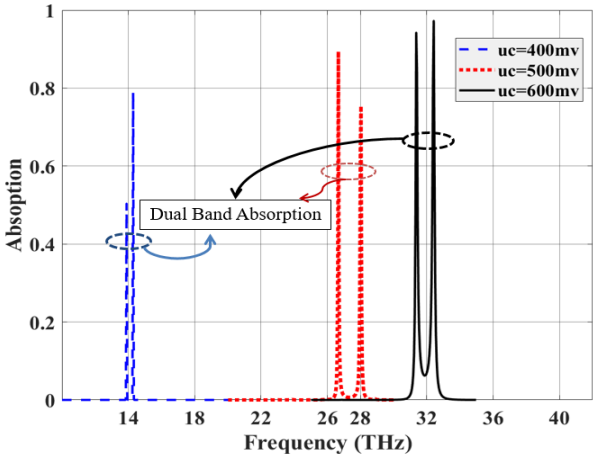

Fig. 2. Simulated absorption spectra for three different graphene chemical potential

length of the inner square ring is $\boldsymbol{b}$ = 28 nm. The lattice periodicity is $\boldsymbol{P}$ = 60 nm.

III. GRAPHENE NANOPARTICLES DESIGN

The absorption coefficient, A, is obtained from the S_{12} and the S_{11}, transmission and reflection coefficients, respectively [40, 41].

$$A = 1 - |S_{12}|^2 - |S_{11}|^2 \tag{3}$$

The transmitted signal can be neglected due to the existence of a thick metal plate at the bottom of the structure. The thickness of this metal slab is more than the skin depth of the incident wave in the frequency range.

The absorptivity of the proposed graphene absorber is intensive to various parameters. Hence, the frequency and peak absorption are influenced by varying these parameters. First, the effect of the initial characteristics of graphene, μ_c, on the performance of the designed absorber, was studied. After that, the absorption of the proposed structure was evaluated based on the permittivity of the graphene substrate. Eventually, the absorbers' behavior in different incident angles, was examined.

A. GRAPHENE CHEMICAL POTENTIAL EFFECT

The absorption coefficient of the proposed structure as a function of the frequency is presented in Fig. 2. It illustrates a dual-band phenomenon in a normally plane wave excitation through three different types of graphene with chemical potential equal to 400 meV, 500 meV, and 600 meV, respectively. The optimization procedure as well as simulated results were performed by full-wave CST Microwave Studio. Therefore, the selected chemical potential range of 0.4–0.6 eV not only represents a practically achievable tuning interval based on typical gate-voltage biasing in graphene-based devices, but also provides effective modulation of the absorption peaks, as demonstrated by the simulation results in Fig. 2. Changing the chemical potential of graphene leads to altering the absorption spectrum, as shown in Fig. 3. By increasing this factor, the absorption frequency is shifted to the higher frequencies with a better absorption rate. The best absorption is achieved upon $\mu_c = 600\ mV$. Fig. 3 illustrates the center frequency variations for different values of chemical potential.

It is evident from Fig. 3 that there is the existence of dual-band absorbers in all three designs. With $\mu_c = 400\ mV$, the absorption factor is nearly 50% and 78% at center frequencies equal to 13.9 THz and 14.3 THz, respectively. Increasing the μ_c yields resonance frequency increment as well as the absorption coefficient. In $\mu_c = 500\ mV$, 97.9% absorption is achieved at 26.7 THz and 95.63% at 28 THz, as shown in Fig. 3b. An acceptable response is achieved at 31.4 THz, absorption 99% and the most absorption 99.63% at 32.4 THz with $\mu_c = 600\ mV$. Therefore, increasing the chemical potential parameter exceeds more absorption factor.

B. INCIDENT WAVE ANGLE EFFECT

For the proposed graphene-doped absorbers, the incident electromagnetic wave is assumed to be a normal incident wave to the graphene lattices. To evaluate the robustness of these absorbers versus the incident wave angle, the second design with $\mu_c = 500\ mV$ has been simulated with different angles of the incident wave as depicted in Fig. 4. The incident wave angle varied from the oblique wave ($\theta = 0^o$) to tangential wave radiation ($\theta = 90^o$).

As displayed in Fig. 4, it is obvious that there is an existence of dual-band absorbers with fixed absorbance frequencies. However, the absorption peaks decrease while the incident wave deviates from the normal emission. The best absorption achieved 97.9% at 26.7 THz in the oblique incident wave.

C. SUBSTRATE ELECTRICAL CONDUCTIVITY EFFECT

The last parameter examined for the proposed structure absorption is the permittivity of the

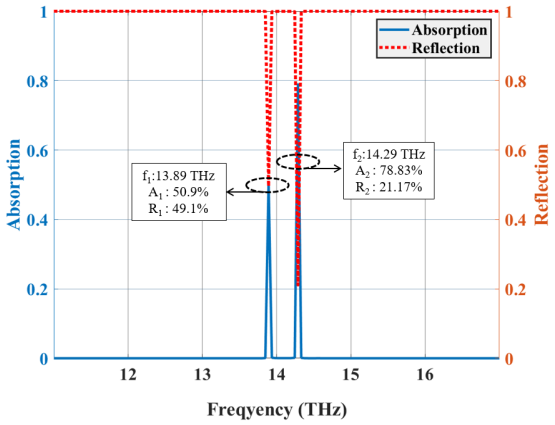

(a)

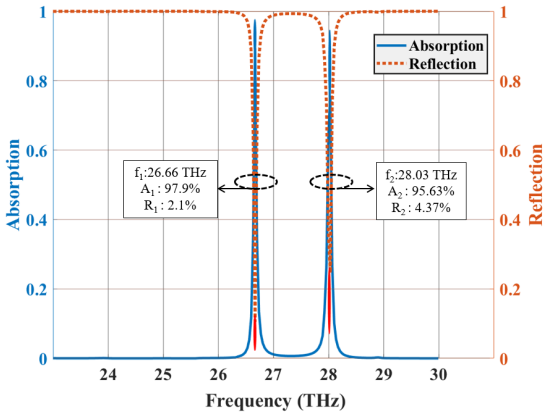

(b)

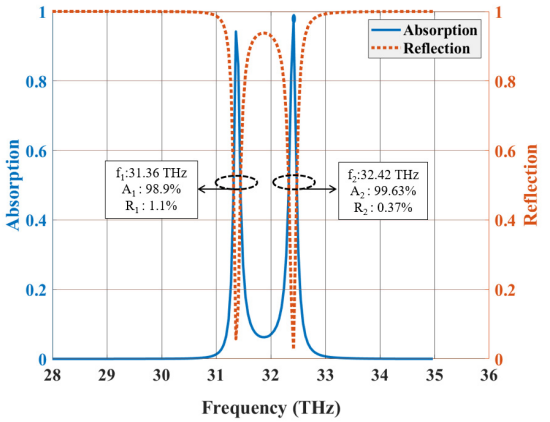

(c)

Fig. 3. The reflection and absorption of the incident wave for different chemical potential values, a μ_c = 400 mV, b μ_c = 500 mV, c μ_c = 600 mV

graphene substrate. Four different materials are compared, including polyamide, silicon dioxide, silicon nitride, and Graphite iron with an equal thickness of 10 nm. In Table 1, the efficiency of proposed dual-band graphene absorbers with $\mu_c = 500\,mV$, designed with a dielectric spacer

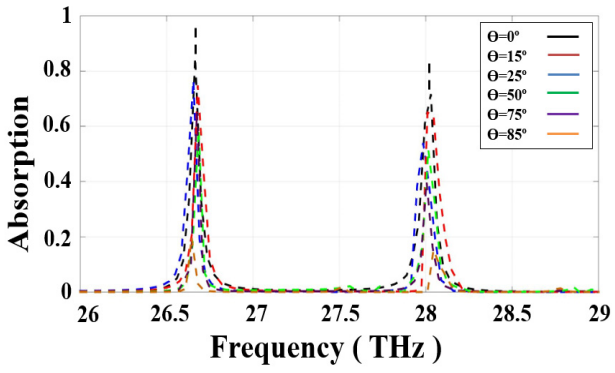

(a)

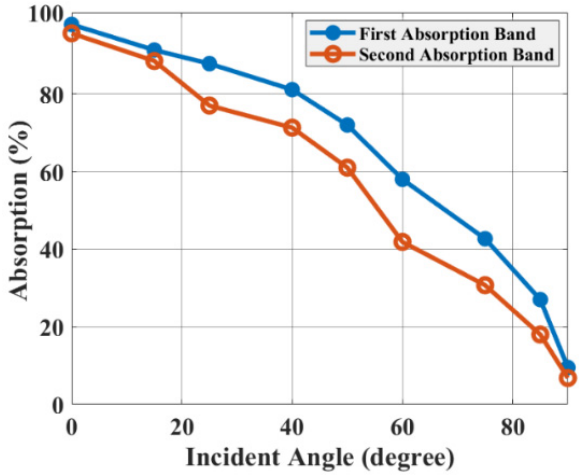

(b)

Fig. 4. Absorption versus incident angle, a Frequency dependence, b Incident angle dependence

Table 1. Performance of different dielectric spacers on the absorption spectra

Substrate Material	Absorption Frequencies	Absorption Coefficient	Absorption Band-Gap	Absorption Spectra
Polyamide $\varepsilon_{r1} = 2$	f1: 26.66 THz f2: 28.03 THz	A1: 84.9% A2: 71.63%	Δf = 1.36 THz	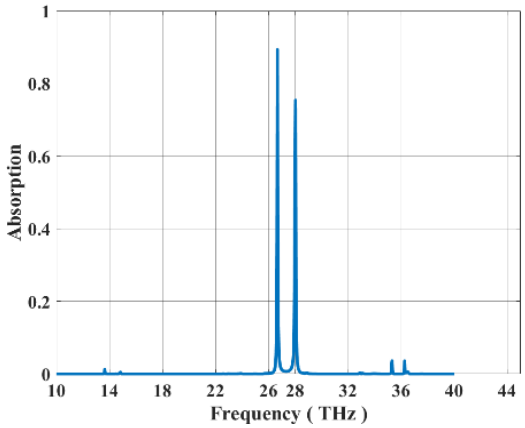

Substrate Material	Absorption Frequencies	Absorption Coefficient	Absorption Band-Gap	Absorption Spectra
Silicon Dioxide $\varepsilon_{r1} = 3.9$	f1: 22.78 THz f2: 25.3 THz	A1: 98.95% A2: 98.48%	Δf = 2.52 THz	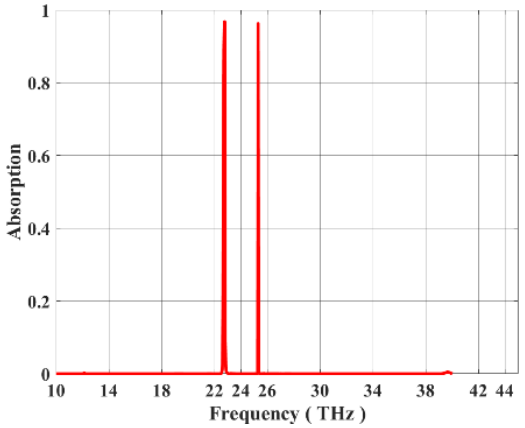
Silicon Nitride $\varepsilon_{r1} = 7.15$	f1:17.18 THz f2:37.9 THz	A1: 98.29% A2: 96.12%	Δf = 20.72 THz	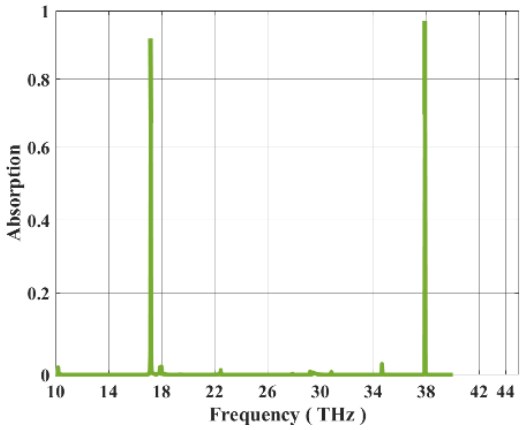
Graphite $\varepsilon_{r1} = 10.3$	f1:15.52 THz f2:41.4 THz	A1: 99.35% A2: 97.84%	Δf = 25.88 THz	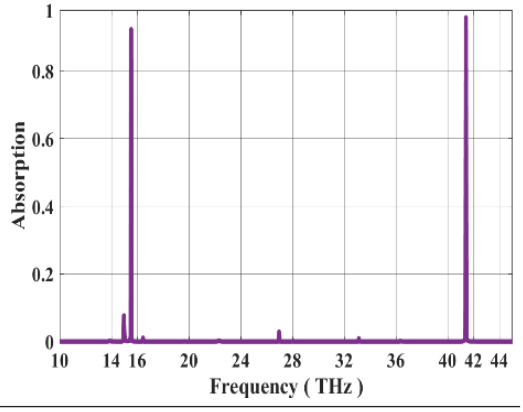

Table 2. Comparison between proposed graphene absorber and previous research

References	Frequency (THz)	Absorption Band No.	Substrate εr	Absorption Peak (%)	Year
[35]	7.628	Single-Band	8.73	99.99	2021
[36]	2.7 - 4.6	4-Band	3.9	99.43	2021
[37]	210.2 - 337.4	4-Band	3.9	99.98	2022
[42]	1.59 - 5.11	5-Band	3	97.35	2020

References	Frequency (THz)	Absorption Band No.	Substrate εr	Absorption Peak (%)	Year
[43]	22.33, 27.59	2-Band	3.9	98.77	2022
[44]	4.24 - 10.62	4-Band	3.9	97.74	2022
[45]	0.3 - 4	3-Band	2	99.3	2023
Proposed	31.36, 32.42	2-Band	12	99.63	-

having diverse dielectric constants, is presented.

The dual-band absorption is prepared in two different THz frequencies, in all structures. The distances between two absorption bands and the peak frequencies are changed with various spacer materials. More distances between two adjacent frequencies are feasible for the increment of the substrate's electrical conductivity.

Actually, increasing the permittivity (ε_r) of the graphene substrate layer, improves the absorption level. In Table 2, the absorber design presented is compared with some other absorbers that have been investigated in recent years.

The proposed dual-band terahertz absorber, exhibiting strong absorption peaks at 31.36 THz and 32.42 THz, with high efficiency exceeding 99%, dynamic tunability via chemical potential control, and angular stability, offers multiple practical applications in emerging terahertz technologies. One of the most promising applications lies in terahertz spectroscopic sensing, where many biological and chemical compounds exhibit distinct spectral signatures within the THz range. The presence of two sharp and tunable absorption bands enables simultaneous or selective detection of multiple target substances. This capability, combined with the angularly stable performance of the structure, supports real-time, robust biosensing and environmental monitoring.

Another key application area is electromagnetic stealth and signature suppression. In this context, the ability of the absorber to eliminate backscattered THz radiation at two critical frequencies makes it highly suitable for stealth coatings on UAVs, antennas, or other surfaces exposed to THz surveillance or radar systems. The compactness and conformal nature of the proposed design further support its integration in real-world stealth applications.

The structure can also serve as a spectral masking element in THz imaging systems. By selectively absorbing specific frequencies, it can enhance image contrast or suppress undesired background responses. This is particularly useful in biomedical and security imaging scenarios where precise spectral filtering is necessary.

Furthermore, the absorber can be applied in selective energy harvesting or THz detection systems. The dual-band high-Q resonance enhances energy capture at target frequencies, and the

tunable nature of the design makes it adaptable for use in frequency-selective detectors or self-powered sensor modules.

Finally, the stable and repeatable spectral response of the structure qualifies it as an effective reference surface for calibration in THz spectroscopy and imaging setups. The dual-band response provides precise benchmarks for validating spectral accuracy in experimental configurations.

IV. CONCLUSION

Dual-band absorbers with high absorbance coefficients are presented in this paper. The investigated structure is composed of two square graphene patches on the substrate. By increasing the chemical potential of the graphene surface, two absorption frequencies of the proposed structure are increased with a better absorption rate. The best absorption, 99.63% is achieved upon $\mu_c = 600\,mV$ at 32.42 THz. The effect of the angle of incident wave on the presented structure with $\mu_c = 500\,mV$ has been examined to evaluate the performance of these absorbers versus the incident wave angle. In this situation, the best absorption achieved 97.9%, at 26.7 THz in the oblique incident wave. The effect of the graphene substrate permittivity was examined. In all structures dual band absorption is prepared in two different THz frequencies. The distances between two absorption bands and the peak frequencies are changed with various spacer materials.

REFERENCES

[1] S. Ma, and S. M. Anlage, "Microwave applications of photonic topological insulators," *Appl. Phys. Lett.,* vol. 116, no. 25, 2020.

[2] A. S. Solntsev, G. S. Agarwal, and Y. S. Kivshar, "Metasurfaces for quantum photonics," *Nature Photon.,* vol. 15, no. 5, pp. 327-336, 2021.

[3] A. Rahim, A. Hermans, B. Wohlfeil, et al, "Taking silicon photonics modulators to a higher performance level: state-of-the-art and a review of new technologies," *Adv. Photon.,* vol. 3, no. 2, pp. 024003-024003, 2021.

[4] C. Trovatello, A. Marini, X. Xu, C. Lee, F. Liu, N. Curreli, C. Manzoni et al, "Optical parametric amplification by monolayer transition metal dichalcogenides," *Nature Photon.,* vol. 15, no. 1, pp. 6-10, 2021.

[5] M. M. Fakharian, "Bilayer reprogrammable graphene meta-atoms for THz wave reflection/absorption," *Opt. Quant. Electron.,* vol. 56, pp. 849, 2024.

[6] M. A. Butt, S. N. Khonina, and N. L. Kazanskiy, "Recent advances in photonic crystal optical devices: A review," *Opt. Laser Technol.,* vol. 142, pp. 107265, 2021.

[7] S. Khani, and M. Hayati, "Optical biosensors using plasmonic and photonic crystal band-gap structures for the detection of basal cell cancer," *Sci. Rep.,* vol. 12, no. 1, pp. 5246, 2022.

[8] A. R. Jalalvand, Z. Rashidi, M. Khajenoori, "Sensitive and selective simultaneous biosensing of nandrolone and testosterone as two anabolic steroids by a novel biosensor assisted by second-order calibration," *Steroids,* vol. 189, pp. 109138, 2023.

[9] G. J. Tang, X. T. He, F. L. Shi, J. W. Liu, X. D. Chen, and J. W. Dong, "Topological photonic crystals: Physics, designs, and applications," *Laser Photon. Rev.,* vol. 16, no. 4, pp. 2100300, 2022.

[10] A. H. Alipour, S. Khani, M. Ashoorirad, et al, "Trapped multimodal resonance in magnetic field enhancement and sensitive THz plasmon sensor for toxic materials accusation," *IEEE Sensors J.,* vol. 13, no. 2, pp. 14057-14066, 2023.

[11] M. M. Fakharian, Design of a terahertz metasurface absorber based on machine learning technique, *Tabriz J. Elec. Eng.,* vol. 54, no. 3, pp. 291-299, 2024.

[12] S. Khani, and M. Hayati, "An ultra-high sensitive plasmonic refractive index sensor using an elliptical resonator and MIM waveguide," *Superlatt. Microstruct.,* vol. 156, pp. 106970, 2021.

[13] S. M. Ebadi, and S. Khani, Design of a tetra-band MIM plasmonic absorber based on triangular arrays in an ultra-compact MIM waveguide," *Opt. Quant. Electron.,* vol. 55, pp. 482, 2023.

[14] P. Li, P.S. Zhang, X.H. Deng, et al, "Tunable multiband metamaterial perfect absorber based on a metal-graphene multilayer structure," *Indian J. Phys.,* vol. 99, pp. 395-401, 2025.

[15] E. Einarsson, and J. Bird. Active plasmonic antenna arrays for terahertz frequency communications," Tech. Rep., AFRL-RI-RS-TR-2023-095, May 2023.

[16] S. M. Hoseini, H. Dehbovid, S. M. A. Pahnehkolaei, et al, "Multi-band THz plasmonic meta-surface absorber based on dual bias graphene disks: Bio sensing application," *Indian J. Phys.,* vol. 98, pp. 4577-4583, 2024.

[17] A. A. Balandin, "Phononics of graphene and related materials," *ACS Nano,* vol. 14, no. 5, pp. 5170-5178, 2020.

[18] S.A. Khatami, P. Rezaei, "Coupled mode theory analysis of the graphene-based multi-band superabsorber for selective sensing application," *Diam. Relat. Mater.,* vol. 158, pp. 112690, Oct. 2025.

[19] S. Hayati, Z. Atlasbaf, C. J. Z. Rodríguez, et al, "Dyadic Green's function for the electrically biased graphene-based multilayered spherical structures," J. *Quantitative Spectroscopy Radiative Transfer,* vol. 256, pp. 107251, 2020.

[20] Q. Zhou, Q. Qiu, and Z. Huang, "Graphene-based terahertz optoelectronics," *Opt. Laser Technol.,* vol. 157, pp. 108558, 2023.

[21] N. Rouhi, C. Santiago, D. Jain, K. Zand, Y. Y. Wang, E. Brown, L. Jofre, and P. Burke, "Terahertz graphene optics," *Nano Res.,* vol. 5, pp. 667-678, 2012.

[22] E. Momeni, H. Yaghobi, and A. Shahzadi, "Using dynamic state estimation to detect loss of excitation in synchronous generators," *IET Generation, Transmiss. Distribut.,* vol. 18, no. 3, pp. 639-652, 2024.

[23] X. Li, J. Yu, S. Wageh, A. A. Al-Ghamdi, and J. Xie, "Graphene in photocatalysis: a review," *Small,* vol. 12, no. 48, pp. 6640-6696, 2016.

[24] W. Choi, I. Lahiri, R. Seelaboyina, and Y.S. Kang, "Synthesis of graphene and its applications: A review," *Critical Rev. Solid State Mater. Sci.,* vol. 35, no. 1, pp. 52-71, 2010.

[25] M. J. Allen, V. C. Tung, and R. B. Kaner, "Honeycomb carbon: A review of graphene," *Chemical Rev.,* vol. 110, no. 1 pp. 132-145, 2010.

[26] M. Amin, O. Siddiqui, H. Abutarboush, M. Farhat, and R. Ramzan, "A THz graphene metasurface for polarization selective virus sensing," *Carbon,* vol. 176, pp. 580-591, 2021.

[27] B. Wang, K. Gai, R. Wang, F. Yan, and L. Li, "Ultra-broadband perfect terahertz absorber with periodic-conductivity graphene metasurface," *Opt. Laser Technol.,* vol. 154, pp. 108297, 2022.

[28] M. Biabanifard, A. Arsanjani, M. S. Abrishamian, and D. Abbott, "Tunable terahertz graphene-based absorber design method based on a circuit model approach," *IEEE Access,* vol. 8, pp. 70343-70354, 2020.

[29] P. Zamzam, P. Rezaei, O. Mohsen Daraei, S.A. Khatami, "Band reduplication of perfect metamaterial terahertz absorber with an added layer: Cross symmetry concept," *Opt. Quant. Electron.,* vol. 55, pp. 391, April 2023.

[30] H. Ahmadi, S. Vaezi, V. Jafarzadeh-Harzand, and R. Safian, "Graphene-based terahertz metamaterial absorber for broadband applications," *Solid State Commun.* vol. 323, pp. 114023, 2021.

[31] B. Khodadadi, M. Babaeinik, V. Ghods, et al, "Triple-band metamaterial perfect absorber for refractive index sensing in THz frequency," *Opt. Quant. Electron.,* vol. 55, no. 5, pp. 431, May 2023.

[32] M. Ghaderi, and P. Rezaei, "Low profile wide band high gain transmitarray antenna for Ku band applications," *Opt. Commun.,* vol. 566, pp. 130701, 2024.

[33] P. Zamzam, P. Rezaei, S.A. Khatami, and B. Appasani, "Super perfect polarization-insensitive graphene disk terahertz absorber for breast cancer detection using deep learning," *Opt. Laser Technol.,* vol. 183, pp. 112246, 2025.

[34] A. Norouzi-Razani, P. Rezaei, P. Zamzam, S. A. Khatami, et al, "Absorption-based ultra-sensitive RI sensor based on the flower-shaped graphene resonator for early detection of cancer," *Opt. Commun.,* vol. 524, pp. 128775, 2022.

[35] P. Zamzam, P. Rezaei, Y. I. Abdulkarim, et al, "Graphene-based polarization-insensitive metamaterials with perfect absorption for terahertz biosensing applications: Analytical approach," *Opt. Laser Technol.,* vol. 163, pp. 109444, 2023.

[36] S. A. Khatami, P. Rezaei, and P. Zamzam, "Quad band metal-dielectric-metal perfect absorber to selective sensing application," *Opt. Quant. Electron.,* vol. 54, no. 10, pp. 638, 2022.

[37] B. Khodadadi, P. Rezaei, and S. Hadipour, Dual-band polarization-independent maze-shaped absorber based on graphene for terahertz biomedical sensing, *Opt. Exp.,* vol. 32, no. 27, pp. 545227, 2024.

[38] K. Ziegler, "Minimal conductivity of graphene: Nonuniversal values from the Kubo formula," *Phys. Rev. B,* vol. 75, no. 23, pp. 233407, 2007.

[39] G.W. Hanson, "Dyadic Green's functions and guided surface waves for a surface conductivity model of graphene," *J. Appl. Phys.,* vol. 103, no. 6, 2008.

[40] P. Yu, L. V. Besteiro, Y. Huang, J. Wu, et al, "Broadband metamaterial absorbers," *Adv. Opt. Mater.,* vol. 7, no. 3, pp. 1800995, 2019.

[41] Y. Ra'di, C. R. Simovski, and S. A. Tretyakov, "Thin perfect absorbers for electromagnetic waves: Theory, design, and realizations," *Phys. Rev. Appl.,* vol. 3, no. 3, pp. 037001, 2015.

[42] B. Wang, Y. He, P. Lou, W. Huang, and F. Pi, "Penta-band terahertz light absorber using five localized resonance responses of three patterned resonators," *Res. Phys.,* vol. 16, pp. 102930, 2020.

[43] Y. Xiang, L. Wang, Q. Lin, S. Xia, M. Qin, and X. Zhai, "Tunable dual-band perfect absorber based on L-shaped graphene resonator," *IEEE Photon. Technol. Lett.,* vol. 31, no. 6, pp. 483-486, 2019.

[44] A. Norouzi-Razani, and P. Rezaei, "Multiband polarization insensitive and tunable terahertz metamaterial perfect absorber based on the heterogeneous structure of graphene," *Optic. Quant. Electron.,* vol. 54, no. 7, pp. 407, 2022.

[45] R. Zheng, Y. Liu, L. Ling, Z. Sheng, Z. Yi, Q. Song, B. Tang, Q. Zeng, J. Chen, and T. Sun, "Ultra wideband tunable terahertz metamaterial absorber based on single-layer graphene strip," *Diam. Relat. Mater.,* vol. 141, pp. 110713, 2024.